Network Dynamics - Homework 3

January 16, 2023

Abstract

In this report, we present our solution to Homework 3. This report is the result of the active collaboration between: Lorenzo Bergadano (s304415), Francesco Capuano (s295366), Matteo Matteotti (s294552), Enrico Porcelli (s296649) and Paolo Rizzo (s301961). For the sake of full reproducibility, we published our code on GitHub at: https://github.com/fracapuano/NetworkDynamics.

1 Exercise 1

During the fall of 2009 there was a large pandemic of the H1N1-virus, commonly known as the *swine-flu*. During this pandemic it is estimated that about 1.5 million people in Sweden were infected. As an attempt to stop the pandemic and reduce excess mortality the government issued a vaccination program beginning in week 40 of 2009. During the weeks that followed they vaccinated more than 60% of the Swedish population.

Here, we will simulate the pandemic with the goal of highlighting how network structure characteristics and disease-dynamics parameters influenced the actual play-out of the 2009 swine-flu pandemic.

All the data regarding the H1N1 pandemic in Sweden during the fall of 2009 have been taken from the a report by the Swedish Civil Contingencies Agency (*MSB*) and the Swedish Institute for Communicable Disease Control (*SMI*).

We carried out the following tasks in the considered setting:

Question (a-1) Simulate a pandemic on a known graph

Question (a-2) Generate a random graph

Question (b) Simulate the disease propagation on a random graph when no vaccines are available

Question (c) Simulate disease propagation on a random graph when vaccination is carried out

Question (d) Estimate the network-structure characteristics and disease-dynamics parameters for the pandemic in Sweden during the fall of 2009

1.1 Question (a-1)

Prior to simulating the pandemic, we built a symmetric k-regular graph $\mathcal{G}$ with $|\mathcal{V}|= 500$ nodes. This type of graph presents a particular structure, as each of its $|\mathcal{V}|$ nodes is connected (in the case in which k is not odd), both leftwards and rightwards, to the $k/2$ nodes whose indices are closer to it.

To simulate the pandemic, we adopted a disease propagation model that well matches various characteristics of the actual outbreak: a discrete-time variant of the well-known SIR epidemic model.

It is indeed the case that as H1N1 did spread, healthy individuals become infected with the virus according (albeit not deterministically) to the number of infected individuals they come in touch with. Moreover, because of aspects of the epidemic that are more related to clinical aspects of the disease, a fraction of these infected individuals would eventually recover, developing antibodies that, at least in the time-frame considered, would make these very individuals immune to the disease.

Considering that casualties due to H1N1 were reported to be less than 0.02 % of the total population [1], they have been considered negligible for this model.

The presence of these three possible states each individual could be in justifies the adoption of the SIR model to describe the 2009 H1N1's pandemic.

If one indicates with $\beta \in [0, 1]$ the probability that in a time unit an already infected individual spreads the disease, infecting a susceptible individual, then the probability that a susceptible individual becomes infected, when it is surrounded by m infected, is $1 - (1 - \beta)^m$, under the reasonable assumption that infected individuals do interact with susceptible ones indipendently one from another.

Formally:

$$\mathbb{P}\left(X_i(t+1) = I | X_i(t) = S, \sum_{j \in \mathcal{V}} W_{ij} \delta^I_{X_j(t)} = m \right) = 1 - (1 - \beta)^m, \quad \forall i \in \mathcal{V} \tag{1}$$

Where here W represents the adjacency matrix of $\mathcal{G}$ and $X(t) \in \mathcal{A}^{\mathcal{V}}$ represents the state of the system at time t. Of course, the state of the system conceptually coincides with a description of the state (either S, I or R) each individual in the population (represented through a node in $\mathcal{G}$) is in.

Above all, equation 1 shows that the probability that an susceptible agent becomes infected clearly depends on topological aspects of the network. This aspect also reflects the quite natural expectation that, as the number of infected individuals among one's contacts increases, so does their probability of contracting the disease. Moreover, as the number of contacts one has increases, so does their probability of being infected, since the probability of being infected grows with m (which is upper bounded by the actual degree of each node).

Let us indicate with $\rho \in [0, 1]$ the probability that one individual recovers during one timestep. Formally,

$$\mathbb{P}(X_i(t+1) = R | X_i(t) = I) = \rho, \quad \forall i \in \mathcal{V} \tag{2}$$

Considering these fundamental aspects, one could, at least in principle, derive an analytical model to describe the evolution of the outbreak. This evolution is described through metrics that typically are the expected number of new infections in each of the considered time units, as well as the expected number of people in each of the three states of the SIR model.

However, while these quantities can be obtained *analytically* for simple epidemics -either because the network has a simpler structure, such as ring or line-like, or the epidemic model is actually simpler, as it might be binary-, in a fairly realistic setting as the one presented here, it is often times impractical to obtain them analytically and easier to simulate averages to approximate expectations.

[1] World-wide statistic, *Reuters*, 2015

It is worth mentioning that obtaining system-wide global metrics descriptive of system analytically requires storing (and manipulating) the matrix:

$$\Lambda^{\text{discr.}} \in \mathbb{R}^{\mathcal{X}\times\mathcal{X}} \tag{3}$$

This matrix is indexed by all possible states of the system and its entries represent the probability of transitioning among different pairs of states $X^{(i)}, X^{(j)}$. Formally:

$$\Lambda^{\text{discr.}}_{x_1,x_2} = \mathbb{P}(X(t+1) = x_2 | X(t) = x_1), \quad \forall x_1, x_2 \in \mathcal{X} = \mathcal{A}^{\mathcal{V}} \tag{4}$$

While $\Lambda^{\text{discr.}}$ can certainly be interesting in settings with a small number of nodes (< 10), for a SIR model on a population consisting of 500 individuals, each state vector $x \in \mathcal{X}$ has approximately 10^{238} components.

Considering this practical aspect, we resorted to adopt a more "localist" view of outbreak evolution, simulating transitions in $\mathcal{X}$ leveraging equations 1 and 2.

To approximate expectations, we carried out a number of independent simulations equal to $N = 100$ and then averaged the results.

Each simulation would start from a different initial configuration $X(0)$ in which $n = 10$ individuals would be uniformly drawn from the population and infected. The system would then be simulated for 15 units of time (in our case, weeks), with values for β and ρ of 0.3 and 0.7 respectively.

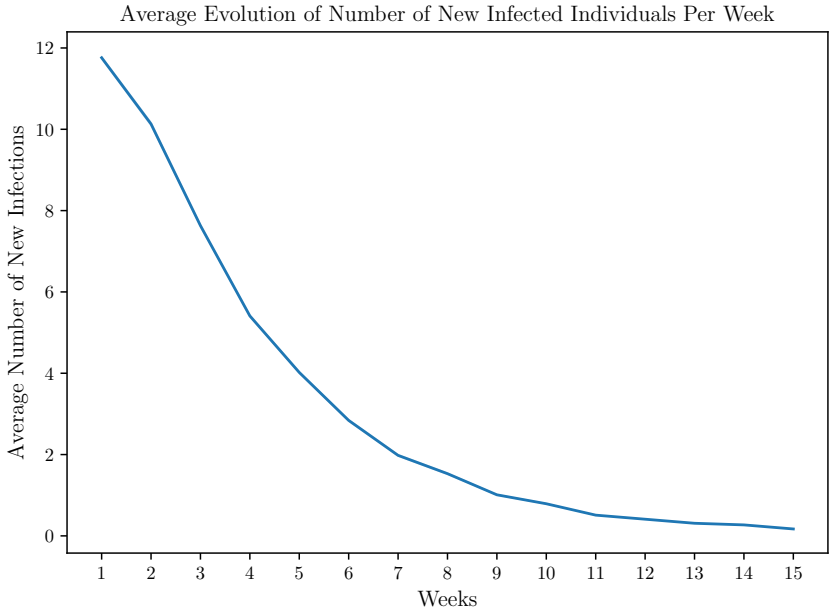

Figure 1: Average (with 95% conf. int.) evolution of the number of new infections

Our results are presented in Figure 1. To test out our hypothesis on the significance of the parameter β in the outbreak evolution, we did run a second simulation with an alternative value of the probability of contracting the infection from one of the neighbours. Figure 2 shows our numerical results.

Moreover, we also show the results of our simulations for what concerns the average evolution of the number of Susceptible, Infected and Recovered individuals comparing the usual values of β and ρ.

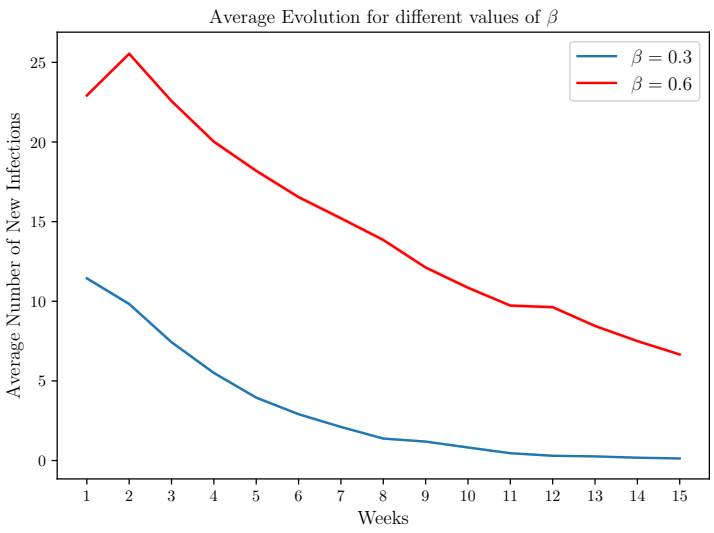

Figure 2: Average (with 95% conf. int.) evolution of the number of new infections for various levels of β

As it is possible to see from Figure 3, the probability of infection clearly is a key driver of the outbreak evolution, as different values of said probability end up panning out very differently.

1.2 Question (a-2)

Random graphs are of great practical interest, as they allow tackling even those problems in which a precise knowledge of the network's topology is not available. This is often the case in many real-world applications.

Social networks, for instance, are typically not fully describable. To require to precisely know that a node $i \in \mathcal{V}$ (representing an individual) is stably connected to other w_i individuals in the network is indeed pretty unrealistic. Moreover, it is often the case that it is too expensive to acquire and/or store the information related to the complete structure of $\mathcal{N}_i^+$ for all i, while it is often much more practical to simply store some statistical properties related to the individuals in the network.

Here, we simulated a random graph according to the preferential attachment model. In this model, nodes are iteratively added to an already existing graph $\mathcal{G}$ until a given condition is met (in our case, we added nodes up to when a the target number 900 individuals was reached). For any $t > 1$, a node i is added to $\mathcal{G}_t$ so that it forms on average $k/2$ links with the other nodes already in a graph. In the preferential attachment model, the probability of the event that n forms a link with a node $v \in \mathcal{V}_t$ depends on the degree of latter: that is, nodes with a higher degree are generally chosen more often than nodes with a smaller one.

We used preferential attachment to simulate a graph with $|\mathcal{V}|= 900$ nodes and an average target degree across nodes equal to $k = 17$, iteratively adding nodes according to the aforementioned procedure to a graph initialized as $\mathcal{G}_0 \equiv \mathcal{C}_{k+1}$, where $\mathcal{C}_n$ represents complete graph with n nodes.

Besides reaching the target average degree, this technique allows to obtain graphs exhibiting a crucial property for simulating social networks: the degree of the nodes in the network follows a power-law distribution (with exponent $\gamma = 3$).

This aspect directly captures a sound hypothesis related to individuals in social networks, as it is

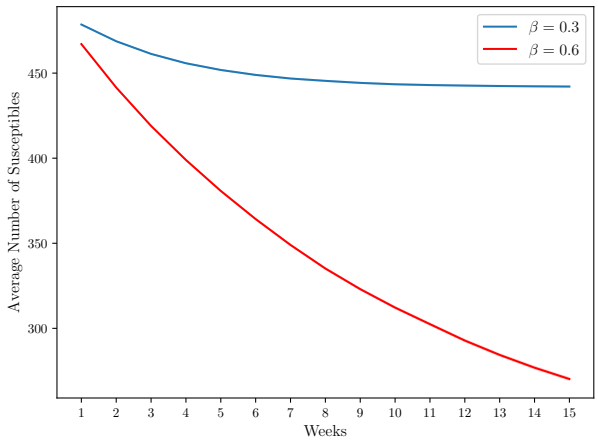

(a) Average evolution of the number of Susceptible individuals over time for various values of β

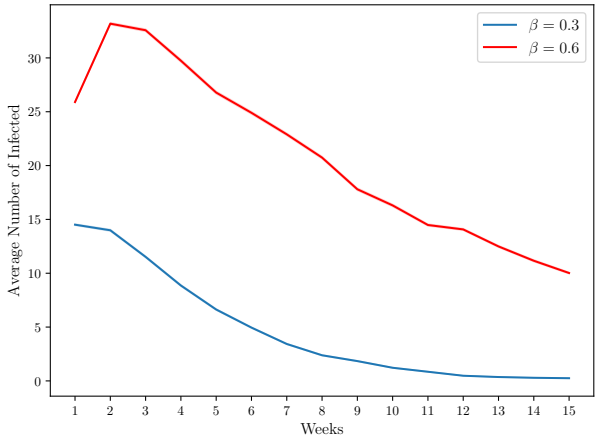

(b) Average evolution of the number of Infected individuals over time for various values of β

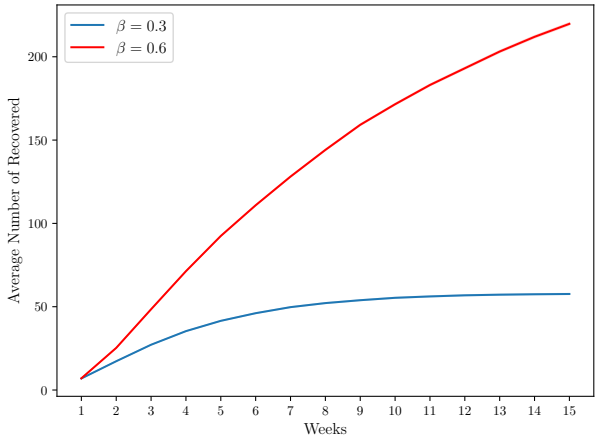

(c) Average evolution of the number of Recovered individuals over time for various values of β

Figure 3: Average System Evolution over 100 simulations (with 95% conf. int.)

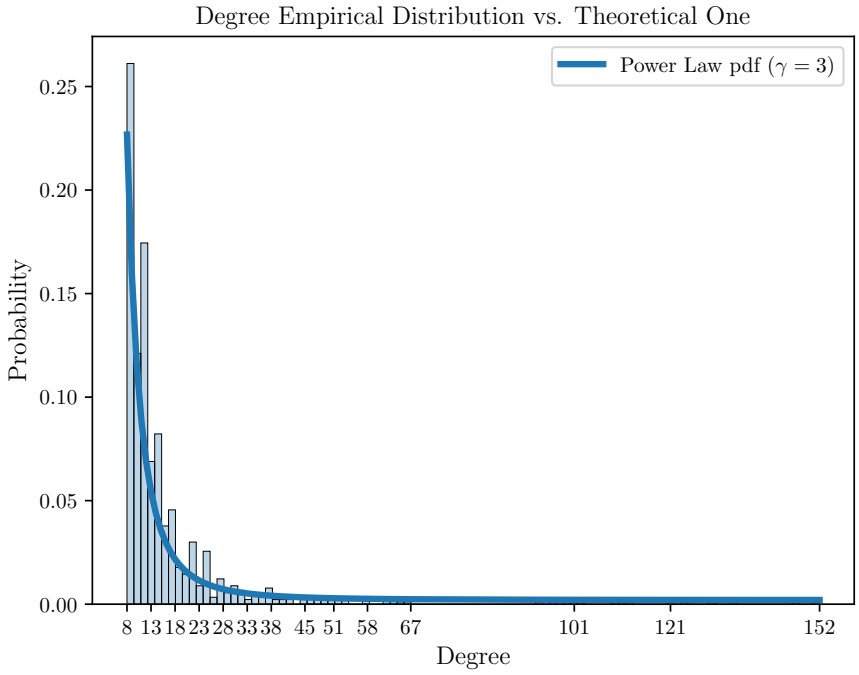

Figure 4: (Empirical) Probability Distribution over nodes' degree in a random graph obtained via preferential attachment

fairly reasonable to expect individuals to have a limited number of connections in the whole network (hence, the distribution of the degree of nodes shall, in principle, be heavily tailed). However, as Figure 5 shows, power-law distributions are particularly interesting as distribution for the degree of nodes since the probability of having nodes with a medium-to-fairly large degree does not decay rapidly as it would do if a node's degree was distributed according to an Exponential with $\lambda = \gamma$, for instance.

Figure 4 shows a comparison between these two alternative distributions.

1.3 Question (b)

Once a stable procedure to obtain random graphs in which nodes have an average degree equal to k is available, one can also simulate epidemics on the results of the application of said technique.

Here, we do simulate a SIR model ($\beta = 0.3$, $\rho = 0.7$) on a randomly generated graph with $|\mathcal{V}| = 500$ nodes and average degree equal to $k = 6$.

The random graph has been obtained according to the aforementioned preferential attachment model, while the outbreak has been simulated starting from 10 infected individuals, drawn at random from the population at the beginning of each simulation. We simulated $N = 100$ trajectories of the epidemics in the configurations space $\mathcal{X}$ and averaged over this simulations to obtain an empirical estimate of the evolution of the number of new infections (Figure 7), Susceptible (Figure 6a), Infected (Figure 6b) and Recovered (Figure 6c) individuals over time.

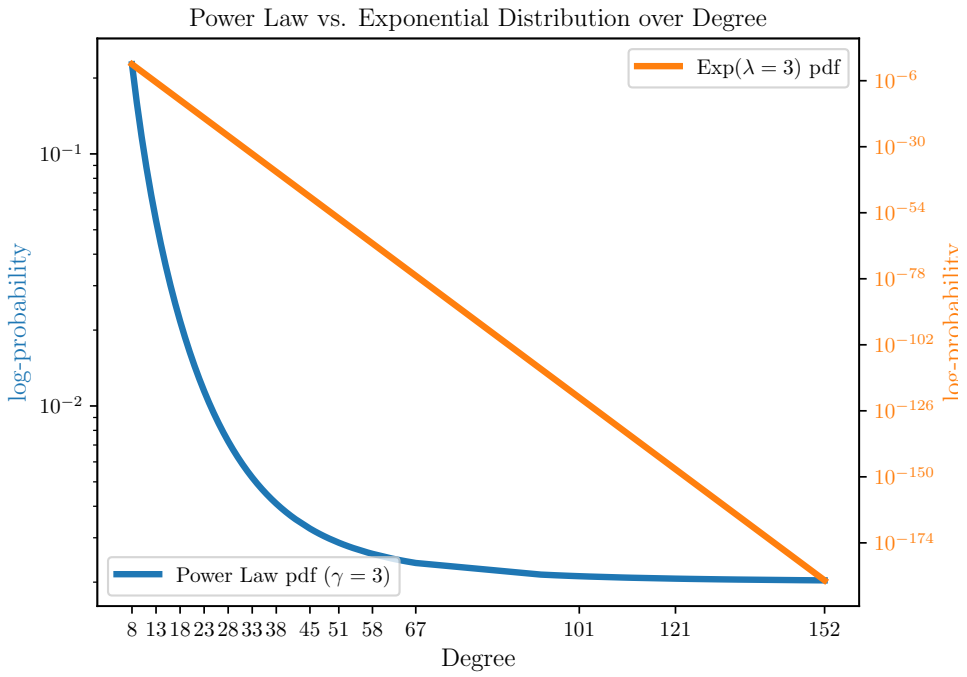

Figure 5: log-pdf of Power-Law distributed Degree vs Exponentially distributed

1.4 Question (c)

To take into account the efforts made by the Swedish Health Service to vaccinate portions of the population against H1N1, we simulated $N = 100$ evolutions of the outbreak taking into account the following vaccination scheme during the 15 weeks we did consider:

$$\text{Vacc} = (0, 5, 15, 25, 35, 45, 55, 60, 60, 60, 60, 60, 60, 60, 60) \tag{5}$$

Figure 8a shows the number of newly vaccinated individuals over time, whereas Figure 8b shows the evolution of the number of individuals that received a jab over time. As expected, both these figures present the informative patrimony conveyed by equation 5.

Vacc is to be interpreted as a vector whose components Vacc_i represent the fraction of the overall population that has already been vaccinated by the i-th week.

In our simulations, vaccines are administered to individuals with the scope of stopping the propagation of the disease. Therefore, we simulated a scenario in which vaccinated individuals can no longer infect others from the moment in which they received their jab.

Also taking into account the mildness of the symptoms [2], people would not be able to exactly tell whether or not they contracted the virus (and therefore, developed or not an autonomous immune response). Considering this aspect, during each week we selected individuals to receive their jab at random (uniformly) in the current population of non-vaccinated, independently on their present state.

Indeed, considering that diagnostics often tend to lose their effectiveness during pandemics, all it mattered for the Health Service was the state of people with respect to being vaccinated.

[2] *John Hopkins Medicine*

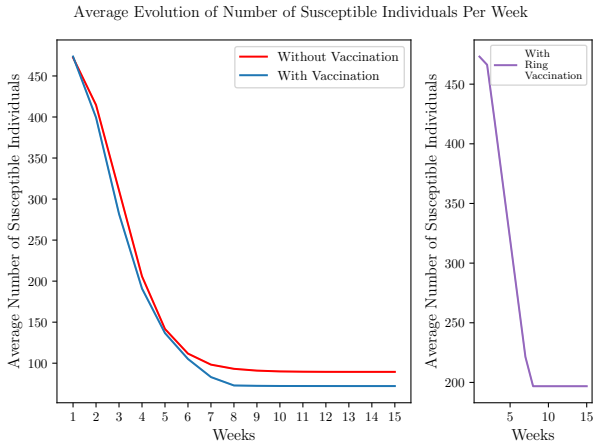

(a) Average evolution of the number of Susceptible individuals over time

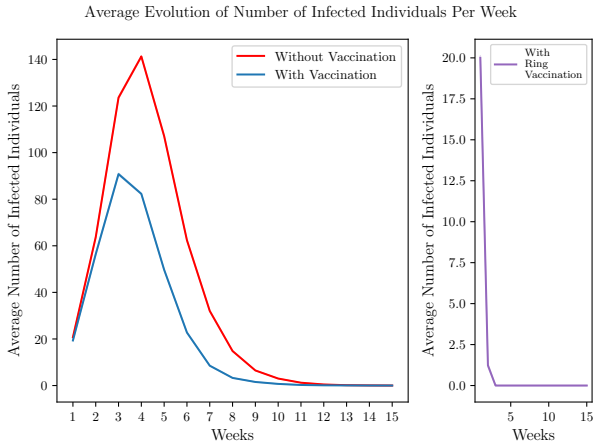

(b) Average evolution of the number of Infected individuals over time

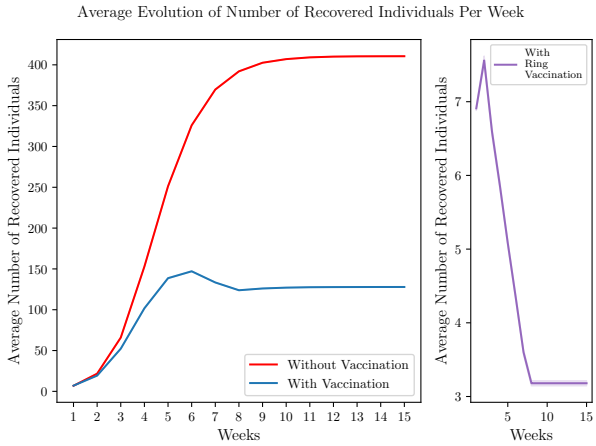

(c) Average evolution of the number of Recovered individuals over time

Figure 6: Average System Evolution over 100 simulations (with 95% conf. int.), with and without vaccinating the population

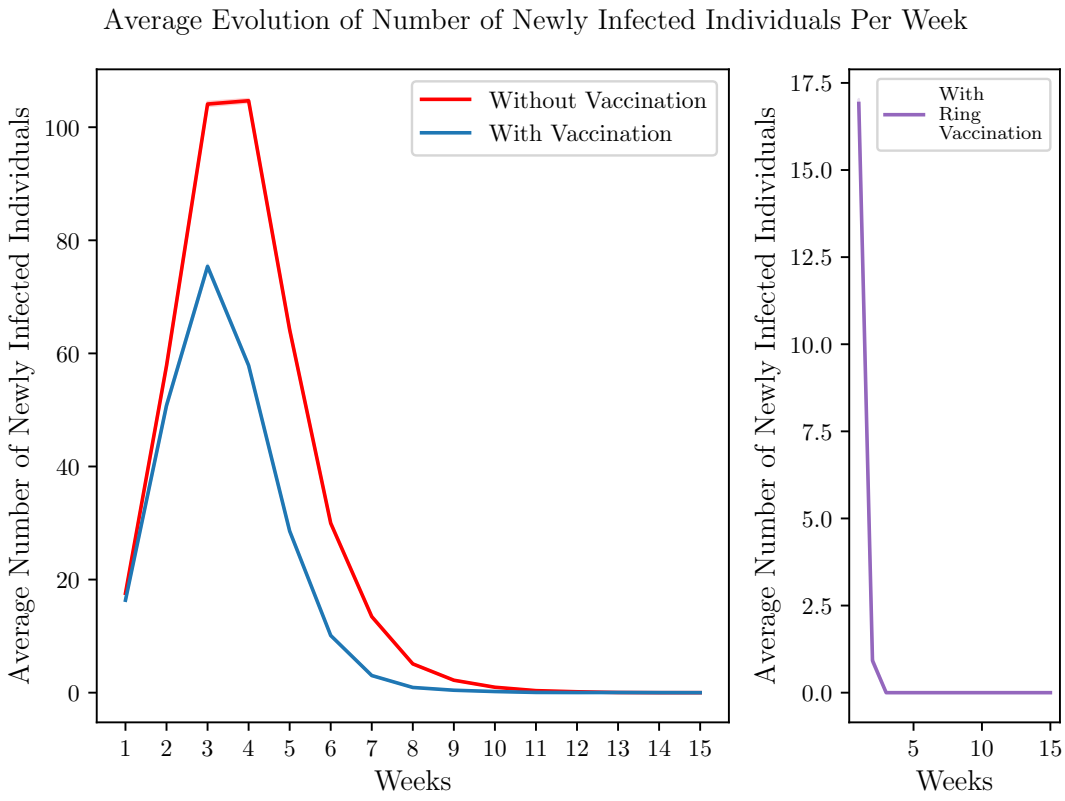

Figure 7: Average (with 95% conf. int.) evolution of the number of new infections, with and without vaccinating the population

We simulated $N = 100$ trajectories of the epidemics in the newly enriched configurations space $\tilde{\mathcal{X}}$ (that does now take into account the "vaccinated" state too) and averaged over these simulations to obtain an empirical estimate of the evolution of the number of new infections (Figure 7), Susceptible (Figure 6a), Infected (Figure 6b) and Recovered (Figure 6c) individuals over time.

Our results prove one very reasonable-to-expect effect of vaccination: the number of new infections during each time frame is dramatically larger in the case in which vaccination is not performed with respect to when it is. To test out our understanding of the effect of the vaccines, we simulated a variant of the system in which individuals are vaccinated according to a probability distribution that favours those individuals having a larger amount of Infected neighbours. In a general sense, this scheme is a noisy variant of the well-known "Ring Vaccination" scheme [3], according to which all the individuals that got exposed to the infection (because of a positive contact) do receive a jab. Jabs are assumed to have the same effect as before.

This scheme is particularly effective in those settings in which the disease morbidity is particularly high (e.g. for the "Ebola" virus) and it has shown to be so promising that represented a key aspect of the strategy for Smallpox eradication.

Although certainly more expensive than a simple random selection process (since the state of each node must be known before-hand at a central level, thus very high costs associated to extensive diagnostic tests and logistics are introduced), ring vaccination has been shown to be certainly very promising in our case too, as it basically led to the extinction of the outbreak in its initial stages.

[3] *Wikipedia*

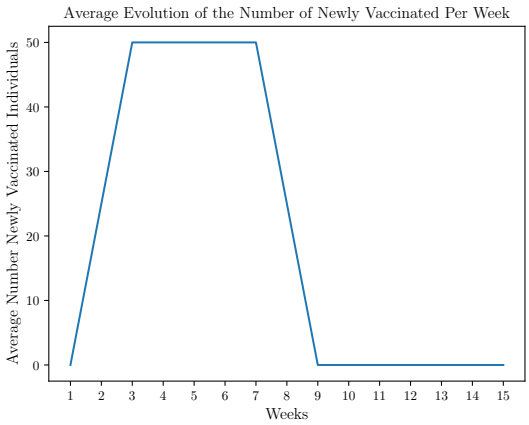

(a) Evolution of the number of Newly Vaccinated Individuals over time

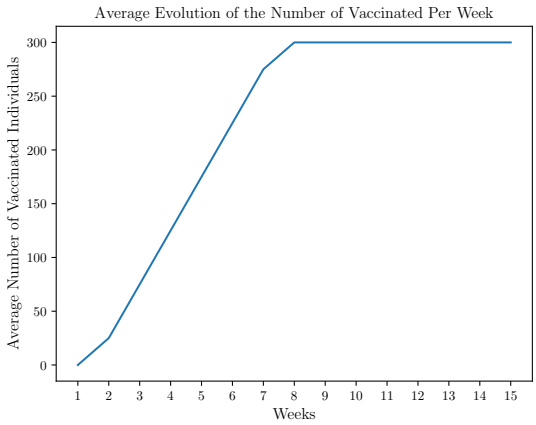

(b) Evolution of the number of Vaccinated Individuals over time

Figure 8: Vaccination Scheme Effects on the number of vaccinated individuals

While random and ring vaccination schemes do vaccinate indeed the same amount of people, by designing the intervention of the network we managed to obtain very different outcomes.

1.5 Question (d)

Albeit their huge potential to allow taking informed decisions, the models just presented obviously suffer from under-modelling. It is indeed the case that many of the assumptions upon which these very models rely are indeed not directly applicable to real scenarios (as, for instance, the behaviour of an agent surrounded by m infected individuals might change as it progressively reckons its situations, thus violating the assumption of independence between the events of contracting the infection from one of its neighbors).

Moreover, it is the case that models do match the intricacies of real-world phenomena to a satisfactory extent. However, often times a precise knowledge of the parameters these very models do rely on is not available. Nevertheless, precise estimates of the parameter set are of great practical (and theoretical) interest: accessing this knowledge paves the way to make predictions and simulate the outcomes of various different scenarios of intervention.

Common techniques to overcome this situation rely on making usage of empirical data collected observing real-world phenomena to tweak the values of the parameters inside a region considered feasible for the same parameters. The data we have been using here has been adapted to a scaled-down version of the Swedish population. In particular, each component of the real-world measurement vector I_0 scales down the real number of new infections by a factor of 10^4. We also did scale down the overall Swedish population to have $|\mathcal{V}|= 934$ nodes only.

The real data measured between week 42, 2009 and week 5, 2010 is:

$$I_0 = (1, 1, 3, 5, 9, 17, 32, 32, 17, 5, 2, 1, 0, 0, 0, 0) \tag{6}$$

Whereas the quota of people that did receive their jab in the same weeks is instead:

$$\text{Vacc} = (5, 9, 16, 24, 32, 40, 47, 54, 59, 60, 60, 60, 60, 60, 60, 60) \tag{7}$$

Let us indicate with $\bar{I}$ the expected evolution of newly infected individuals that one does obtain when simulating the system (as it has been done in 1.4) with parameters k, β and ρ. Clearly enough:

$$\bar{I} = \bar{I}\underbrace{(k, \beta, \rho)}_{x} = \bar{I}(x) \tag{8}$$

However, the dependency between x and $\bar{I}$ has no clear (nor practical) functional form and it can only be estimated simulating the system parameterized by x. Moreover, because of the aforementioned issues in handling $\Lambda^{\text{disc.}}$, one can really only approximate the expected evolution averaging over simulations (in this case, we averaged over $N = 10$ simulations).

If one aims at finding the parameters that best turn out to be inducing a measured real world trajectory, it clearly aims at solving:

$$\begin{aligned} \min_{x} \quad & L(\bar{I}(x), I_0) \\ \text{s.t.} \quad & x \in \mathcal{F} \end{aligned} \tag{9}$$

With $L(\cdot, \cdot) \mapsto \mathbb{R}^+$ being an appropriate loss function for the problem at hand and

$$\mathcal{F} = \bigcap_{i \in [k, \beta, \rho]} \mathcal{F}_i$$

Where $\mathcal{F}_i$ is the feasible region for the i-th parameter.

We did solve Problem 9 using an iterative algorithm that at any given iteration j would essentially try out every parameter configuration (in a grid-search fashion) in a set $\mathcal{S}_j \subseteq \mathcal{F}$ of the form:

$$\mathcal{S}_j = \{c_j - \Delta_j s, c_j, c_j + \Delta_j s\} \tag{10}$$

Over iterations, the "center" of $\mathcal{S}_{j+1}$ would be updated to the $x_j^+ \in \mathcal{S}_j$ that yielded the smallest value of objective function, whereas we chose to set $\Delta_{j+1} s = \frac{\Delta_j s}{2}$, $\forall j$. This algorithm would eventually declare a stoppage when Δ_j goes under a specified threshold (for us, 10^{-5}). Let $w = 16$ be the number of simulated weeks. Then, our loss function is:

$$L(\bar{I}(x), I_0) = \frac{1}{w^2} \|\bar{I}(x) - I_0\|_2 \tag{11}$$

Figure 9 shows the results of our numerical simulation, starting from an initial configuration drawn at random (β and ρ were drawn at random in the $[0, 1]$ range, whereas k was drawn at random in the $[5, 15] \cap \mathbb{Z}$ range).

To limit the bias deriving from the choice of x_0 we repeated the optimization process $J = 5$ times and then selected $x^* = \max_{h=1,\dots,J}\{x_h^*\}$. While this choice significantly increases the computational effort needed to obtain a solution, we believe it can significantly benefit the stability of our solution.

Our predicted evolution has been drawn from the said x^*, i.e.:

$$x^* = \begin{pmatrix} k^* \\ \beta^* \\ \rho^* \end{pmatrix} = \begin{pmatrix} 3 \\ 0.44719 \\ 0.06545 \end{pmatrix} \tag{12}$$

For our solution, we found $L(x^*) \simeq 5.58$. The average evolution (over $N = 10$ simulations) of Susceptible (10a), Infected (10b) and Recovered (10c) individuals is presented in Figure 10.

As it is possible to see, the spread across the mean for this simulation is quite wide. This is most likely due to the fact that $\bar{I}(x)$ is estimated on $N = 10$ simulations only to keep the run-time of the algorithm under bearable time.

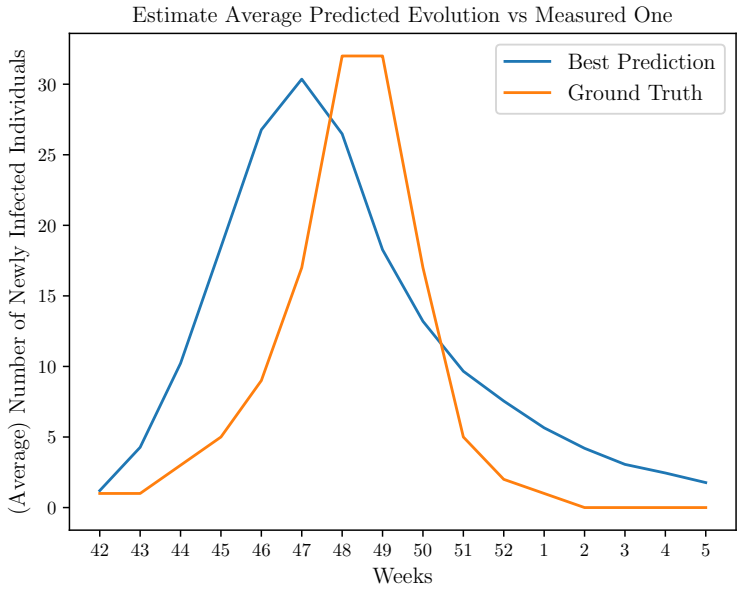

Figure 9: Predicted vs True Evolution of the number of Newly Vaccinated Individuals over time

This implies that, by construction, the algorithm might have converged to a region in which smaller values of objective function were due to a higher statistical variability (intrinsic in the parameters) rather than to the actual goodness of the probed solution x.

1.6 Challenge: A different algorithm to solve Problem 9

As it is possible to derive from the its description, the algorithm just presented operates restricting the feasible region based on the performance of certain x_j. The way contractions of $\mathcal{F}$ are operated heavily relies on the estimate of the current best solution which, given the computational burden associated to simply simulate the system's evolution, might be not very practical. It is indeed the case that the number of function evaluations required by the algorithm presented in 1.5 is $\mathcal{O}(J \cdot 27\text{it})$, with "it" representing the number of iterations the algorithm runs.

Since this value is considerably large, we considered adopting a black-box optimization technique renowned to be particularly sample efficient: Bayesian Optimization (BO)[4]. Since BO probes point at random in $\mathcal{F}$, the number of function evaluations required by this solution is $\mathcal{O}(\text{it})$ that is, more than one order of magnitude smaller than the one required by the previous algorithm.

For the sake of transparency, we report that the results we obtained using this technique (using Upper Confidence Bound as acquisition function and with $\kappa_0 = 5$, exponentially decaying over iterations according to $\kappa(t) = 0.99^t \kappa_0$) were not satisfactory at all.

We believe this to be due due to two main aspects:

- Albeit being very adaptive to all discrete and continuous settings, BO may need an extensive fine-tuning when mixed problems are provided (as was this one, in which some parameters did change in a discrete setting while others did in a continuous one).
- Practically speaking, BO performs the best when it is used on variables in a predefined range (typically, $[0, 1]$). While β and ρ are inherently in this range, k can be mapped to

[4] "*Bayesian Optimization: Open source constrained global optimization tool for Python*"

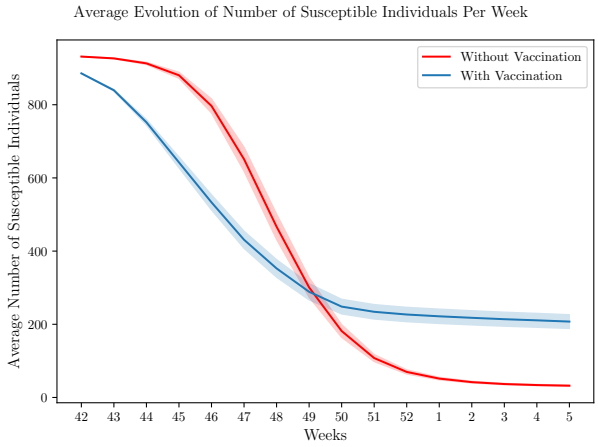

(a) Average evolution of the number of Susceptible individuals over time

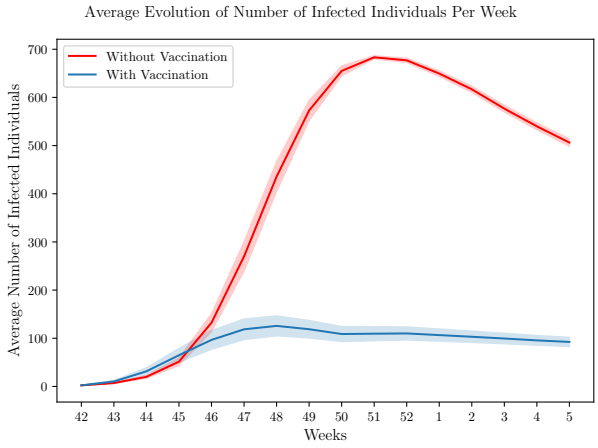

(b) Average evolution of the number of Infected individuals over time

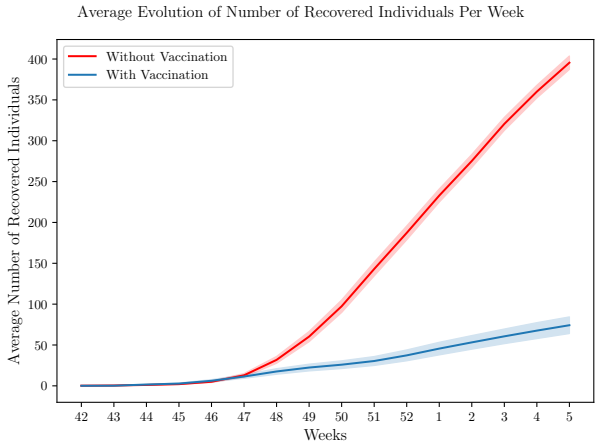

(c) Average evolution of the number of Recovered individuals over time

Figure 10: Average System Evolution over 10 simulations (with 95% conf. int.) obtained with x^*, both with and without vaccinations

numerical values in $[0, 1]$ only through min-max scaling. However, this would inevitably bias the optimization of k, as all the (plausible) values larger than $k_{\max}$ would not be tested.

Finally, it is worth mentioning that probably other choices of L could be explored. It is indeed the case that curves with very low RMSE might still be very sub-optimal. Because of that, BO could receive a biased signal of performance for outbreak simulations that, for instance, perfectly match the right-tail of the evolution but completely miss the peaks (we believe the same holds for 1.5).

Nevertheless, this algorithm could still be used to identify some promising regions in which one might unleash the adaptive grid-search algorithm previously presented. Under the assumption that, at least, BO can cut off some regions of $\mathcal{F}$ which are definitely not promising, this hybrid solution would require a smaller number of iterations with respect to the one presented in 1.5.

2 Exercise 2

In this part, we will study graph coloring as an application of distributed learning in potential games. The aim of graph coloring is to assign a color to each node in a given undirected graph, such that none of the neighbors of a node have the same color as that node. We will begin with a simple line graph to illustrate the distributed learning algorithm, and then look at a more general example, which can be seen as a distributed solution approach to assign non-interfering channels to wifi access points.

Question (a) Study a Noisy Best Response (NBR) dynamics over a line graph with 10 nodes

Question (b) Study a NBR dynamics over a wifi network

Question (c) Test different values of the inverse noise parameter $\eta(t)$

2.1 Question (a)

Following the the problem specification, the simulation starts with $X_i(t) = \textit{red}, \quad \forall i = 1, \dots, 10$ and the updating node is chosen among all the nodes of the graph by following a uniform probability distribution. The new color of the drawn node is chosen according to the following conditional probability:

$$\mathbb{P}(X_i(t+1) = a | X(t), I(t) = i) = \frac{e^{-\eta(t) \sum_j W_{ij} c(a, X_j(t))}}{\sum_{s \in \mathcal{C}} e^{-\eta(t) \sum_j W_{ij} c(s, X_j(t))}} \tag{13}$$

Where $I(t)$ represents the random draw (from a uniform distribution over the nodes) of the node to be updated and $c(s, X_j(t))$ is cost function, defined as:

$$c(s, X_j(t)) = \begin{cases} 1, & \text{if } X_j(t) = s \\ 0, & \text{otherwise} \end{cases} \tag{14}$$

From equation 13 it is clear to derive that as the inverse noise parameter increases (i.e., $\eta \to \infty$) the invariant distribution of the NBR dynamics tends to a uniform probability distribution over the solutions of

$$\arg\min_{x \in \mathcal{X}} \; U(t) \tag{15}$$

where $U(t)$ is the potential function. Clearly enough, from the interpretation of equation 14, here we aim at minimizing the potential function. In our case case:

$$U(t) = \frac{1}{2} \sum_{i,j \in \mathcal{V}} W_{ij} \cdot c(X_i(t), X_j(t)) \tag{16}$$

This function has two minima that are obtained with configurations in which the two possible states are alternating along the nodes of the line. For this reason the invariant distribution probability will be equally concentrated in said configurations and one of them will be observed with very high probability in the 10^4 iterations the algorithm runs.

Our results are shown in Figure 11 and Figure 12. In the first image we can see, as expected, that the resulting coloring pattern is the well known pattern for lines, with two colors alternating along the nodes of the graph.

As highlighted in Figure 12b, an optimal configuration (i.e., one that minimises the potential function) is hit twice during the course of the simulation. The first time is around iteration 100, but since t is not large enough yet, the noise is still high and the probability of escaping from the configuration is still not negligible. For this reason, a change in the value of the potential function (thus in the coloring scheme) according to the Noisy Best Response Dynamics is still plausible. This is exactly what happens in the following iterations, where the network escapes from the optimal configuration and the potential function starts its errating pattern once again.

It eventually hits 0 for the second time around iteration 300. At that point, the value of t is large enough and the dynamics is much less ergodic with respect previous stages of the simulation. As shown in Figure 12a, the simulation remains in an optimal configuration for the remaining iterations. It must be noted that the probability of changing configuration is very close to 0, even though it is not exactly null.

In a sufficiently high constant noise NBR dynamics, if we let the simulation run for an infinite amount of time and compute the fraction of time spent in each state, we should observe a value close to 0.5 for both the optimal configurations. We can not appreciate this behaviour in our simulation due to the nature of the inverse noise parameter $\eta(t)$, which is an increasing function of t. For this reason this particulare NBR dynamics tends to a best response one as $t \Longrightarrow \infty$.

The time needed to pass from one optimal configuration to another, becomes very high as $\eta(t)$ increases because the two optimal configurations are not connected via a direct link in the configuration network and hence the change from one to another would require a momentary loss of potential, which corresponds to a choice that the players tend to avoid when the noise is low.

2.2 Question (b)

Following the problem specification, we simulated a learning dynamics from two different starting configurations over the course $N = 5 \cdot 10^3$ iterations. The starting configurations are:

- *"all red"*. Every node has state "red";
- *"random color"*. Every node has a color drawn from an uniform probability distribution defined over the discrete set of possible colors.

We present one of the two resulting coloring schemes in Figure 13. Due to the high number of colors, a visual verification of this solution may result difficult to the reader. To overcome this problem, the graph of the complete evolution of the potential function has been presented in 14 and it is proof that the obtained solution has near-zero potential (in case of the coloring result in Figure 13, the potential is equal to 4 for both starting configurations). It must be noted that the

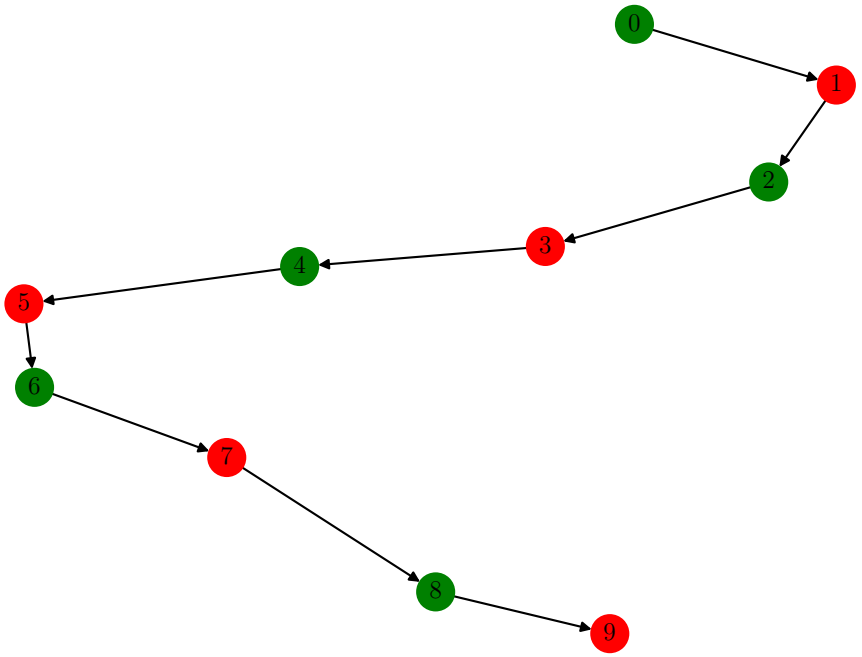

Figure 11: Coloring result of the simulation

optimal configuration is not unique but in the configuration network the optimal solutions are more well connected with respect to the ones found in 2.1

For this reason, although the potential function has remained equal to 4 for several thousands of iterations, the configuration of the network has changed in that time. As stated in the previous exercise, the invariant distribution of this NBR dynamics is a uniform distribution among all the optimal configurations (i.e., the ones satisfying equation 15).

This implies that as the number of iterations grows, the fraction of times that the network has reached any of the given optimal configurations will tend to a probability given by the aforementioned uniform distribution.

2.3 Challenge: Experiment Noisy Best Response with different $\eta(t)$

Here, we study what happens to the Wi-Fi coloring problem with various choices of the inverse-noise parameter η. In particular, we experimented with the following alternatives:

1. $\eta_1(t) = 0,\ \forall t$. In this case, players choose an action independently from the actual payoff it yields;

2. $\eta_2(t) = 3,\ \forall t$, i.e. η is a small constant. Therefore, noise is very effective and the players will choose almost at random but with a small bias towards the best choices;

3. $\eta_3(t) = 100,\ \forall t$, i.e. η is a large constant. which very much limits the noise effect;

4. $\eta_4(t) = \frac{t^4}{100}$ which translates into a rapidly decreasing noise. At every step the player will tend to play the best response with a higher and higher probability over iterations;

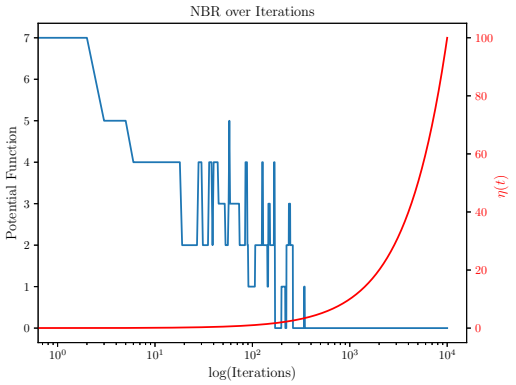

(a) Evolution of the potential function over iterations

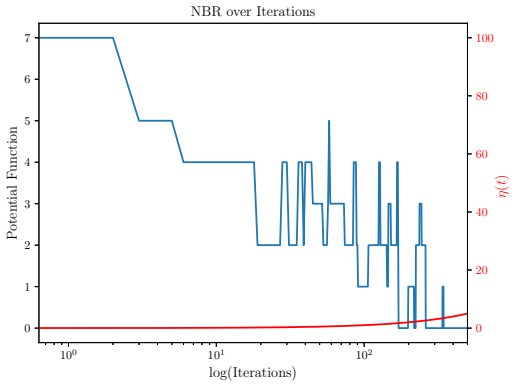

(b) Evolution of the potential function in the first 500 its

Figure 12: Potential Function Evolution with NBR Dynamics on line graph (starting in all red)

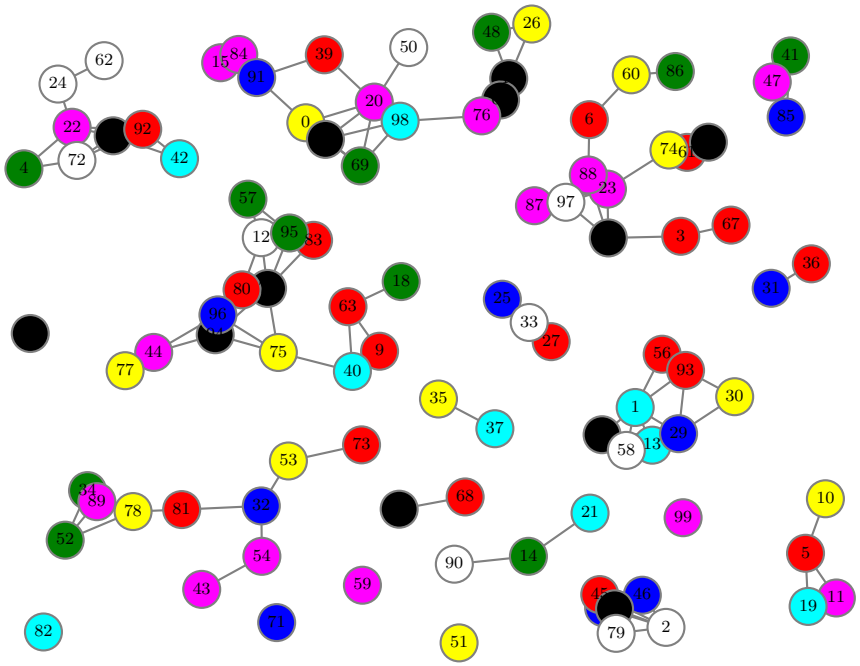

Figure 13: Coloring result of the simulation

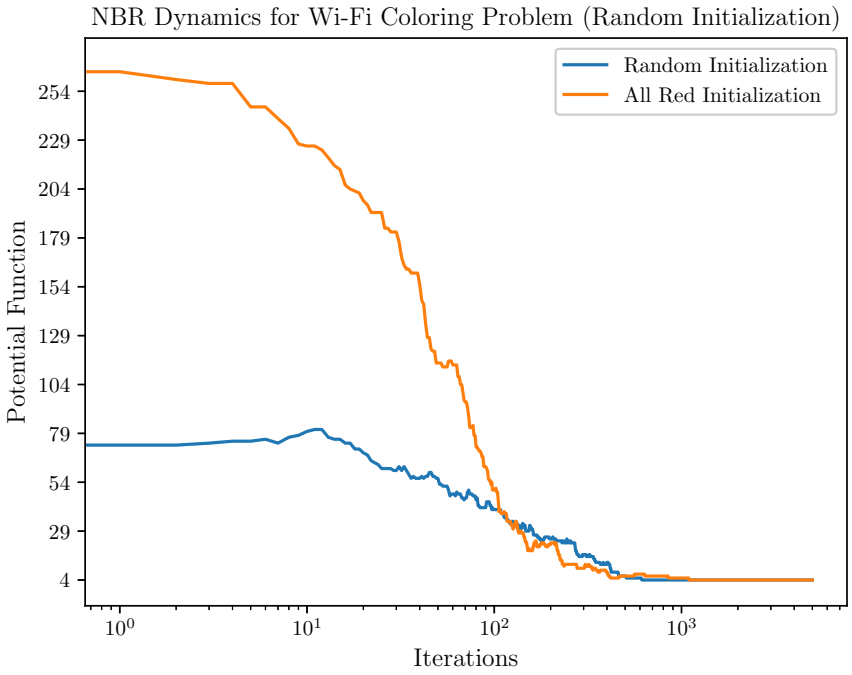

Figure 14: Noisy Best Response Dynamics ($\eta(t) = \frac{t}{100}$)

Our numerical results are presented in Figure 15. As expected, the behaviour of the third and fourth dynamics is quite similar to the one seen in 2.2, although convergence is slightly faster for $\eta_4(t)$ than $\eta_3(t)$.

This matched our expectations, since:

$$\eta_3(t) \leq \eta_4(t) \quad \forall t \geq 10$$

Opposite to what presented in 2.2, it holds true that for the fourth simulation $\frac{t^4}{100}$ grows bi-quadratically rather than linearly (as did $\frac{t}{100}$). Therefore, the NBR dynamics will start behaving approximately as a BR one after fewer iterations (since the noise decays much faster).

More interesting insights can be derived from the results of the first and second dynamics simulated.

With $\eta_1(t)$, the noise is at its maximum and the players are not taking into account the payoff when making a choice. This explains the erratic behaviour seen in the corresponding plot (top-left in Figure 15) and motivates the fact that the potential function actually never stabilizes in its minimum value.

Since $\eta_1(t) = 0$ corresponds to uniform random choices by the players, also the colors are expected to follow a uniform random distribution after a sufficient burn-in phase (the starting point is not random and has influence over the first iterations).

With this simulation we also offer an empirical confirmation to the theoretical result regarding the expectation of the potential function. This can be calculated by using the linearity of expectations:

$$\mathbb{E}[U(t)] = \frac{1}{2} \sum_{i,j \in \mathcal{V}} W_i j \mathbb{E}[c(X_i(t), X_j(t))] \tag{17}$$

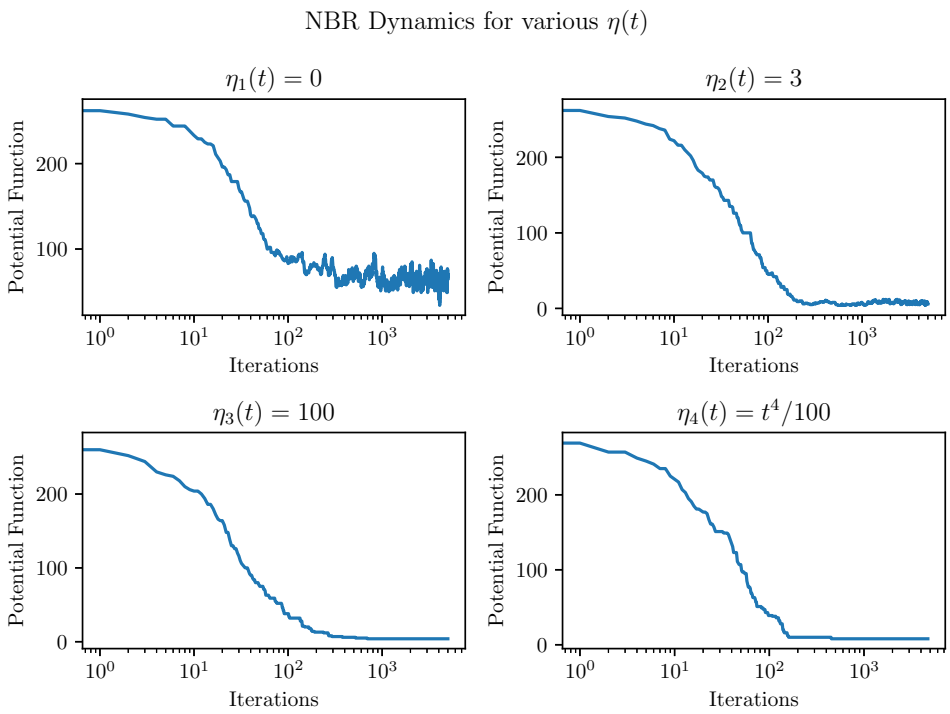

Figure 15: Noisy Best Response for various choices of $\eta(t)$

This calculation translates into the problem of computing the expectation of the cost function, i.e. the average contribution of every link to the potential function. This, by definition, is equal to:

$$\begin{aligned}\mathbb{E}[c(X_i(t), X_j(t))] &= 2 \cdot \mathbb{P}(X_i(t) = X_j(t)) + 1 \cdot \mathbb{P}(|X_i(t) - X_j(t)| = 1) \\ &= 2 \cdot \mathbb{P}(X_i(t) = X_j(t)) + 1 \cdot \mathbb{P}(X_j(t) = X_j(t) + 1) + 1 \cdot \mathbb{P}(X_j(t) = X_j(t) - 1) \\ &= 2 \cdot \frac{1}{8} + \frac{7}{64} + \frac{7}{64} = \frac{15}{32}\end{aligned} \tag{18}$$

Which (equation 17) yields:

$$\begin{aligned}\mathbb{E}[U(t)] &= \frac{1}{2} \sum_{i,j \in \mathcal{V}} W_{ij} \mathbb{E}(c(X_i(t), X_j(t))) \\ &= \frac{1}{2} \cdot 274 \cdot \frac{15}{32} = 64.22\end{aligned} \tag{19}$$

The observed mean is 64.6, which is pretty close to the expected value considering the inflation caused by the "all red" starting configuration, which yields high potential configurations for the first couple hundreds of iterations.

As the value of $\eta(t)$ increases, the expected value of the potential function will reduce. This finds confirmation in our experiments with $\eta_2(t)$ (top-right of 15). In this case, the potential function shows much less fluctuation and the observed average is 10.1 which is much closer to the empirical minimum obtained in 2.2.